Phonons, rotons, and localized Bose-Einstein condensation in liquid He 4 confined in nanoporous FSM-16

Jacques Bossy, Jacques Ollivier, H. Glyde

Phonons, rotons, and localized Bose-Einstein condensation in liquid ^{4}He confined in nanoporous FSM-16

Jacques Bossy,[1] Jacques Ollivier,[2] and H. R. Glyde[3]
[1]*Institut Néel, CNRS, Université Grenoble Alpes, BP 166, 38042 Grenoble Cedex 9, France*
[2]*Institut Laue-Langevin, BP 156, 38042 Grenoble, France*
[3]*Department of Physics and Astronomy, University of Delaware, Newark, Delaware 19716-2593, USA*

(Received 4 January 2019; published 22 April 2019)

We present neutron scattering measurements of the phonon-roton and layer modes of liquid helium confined in 28 Å diameter nanopores of FSM-16. The goal is to determine the energy, lifetime, and intensity of the modes as a function of temperature. It is particularly to determine the highest temperature, denoted T_{PR}, at which well-defined phonon-roton modes are observed at higher wave vector ($Q > 0.8$ Å^{-1}) in the nanopores. The temperature T_{PR}, which can be identified with loss of Bose-Einstein condensation (BEC), can be compared with the superfluid to normal liquid transition temperature, T_O, and other transition temperatures of ^{4}He in the nanopores. The aim is to identify the nature of BEC in a narrow nanopore. Two pressures are investigated, saturated vapor pressure (SVP) and $p = 26$ bars. We find that well-defined P-R modes are observed up to temperatures much higher than the conventional superfluid to normal liquid transition temperature, T_O, observed in torsional oscillator measurements, i.e., $T_{PR} > T_O$. At SVP, $T_{PR} = 1.8$ K and $T_O = 0.9$ K. This supports the interpretation that BEC exists in a localized or partially localized form in the temperature range $T_O < T < T_{PR}$; i.e., there is a localized BEC region lying between the superfluid and fully normal liquid phase, as observed in some other porous media. At close to full filling, the P-R mode energies in FSM-16 are similar to those in bulk liquid ^{4}He. However, a substantial P-R mode width at $T \to 0$ K and at higher temperatures is observed.

DOI: 10.1103/PhysRevB.99.165425

I. INTRODUCTION

Superfluidity of liquid ^{4}He confined in porous media has a rich history of interest [1–3] going back to the 1950s. In confinement, the superfluid fraction, ρ_S/ρ, near the critical temperature for superflow, T_C, can be represented by the same expression as in bulk liquid ^{4}He, $\rho_S/\rho = (1 - T/T_C)^\gamma$, where γ is the critical exponent. In larger pore media such as aerogel, Vycor [mean pore diameter (MPD), $d = 70$ Å], and xerogel, confinement suppresses T_C somewhat below bulk liquid value T_λ with $T_\lambda = 2.172$ K at saturated vapor pressure (SVP), e.g., $T_C = 1.95$–2.05 K in Vycor [4–6] at SVP. The critical exponent usually differs from the bulk value, $\gamma = 0.67$, but is found to be the same in Vycor [2,4]. In smaller pore media such as gelsil (MPD $d = 25$ Å), T_C is suppressed well below T_λ (e.g., $T_C = 1.4$ K at SVP in gelsil) [7,8]. In addition, the phase diagram has been determined as a function of both pressure and temperature [7,8]. At higher pressures, T_C may even go to zero. The pores in Vycor and gelsil are interconnected. At full filling of the pores, confined liquid ^{4}He behaves like an interconnected 3D fluid [2].

Equally interesting are the phonon-roton (P-R) modes [6,9–18] and Bose-Einstein condensation (BEC) in liquid ^{4}He in porous media. In the superfluid phase of bulk liquid ^{4}He, where BEC and superfluidity coexist, well-defined P-R modes are observed at wave vectors out to $Q = 3.6$ Å^{-1}. However, in the normal liquid phase of bulk liquid ^{4}He, $T \geqslant T_\lambda$, well-defined modes are observed at wave vectors in the phonon region only, $Q \leqslant 0.8$ Å^{-1}; i.e., a sound mode only is observed as in other normal liquids. In the normal liquid phase, where there is no BEC, only broad response in the dynamical structure factor, $S(Q, E)$, is observed at higher wave vectors $Q \geqslant 0.8$ Å^{-1}.

In contrast, liquid ^{4}He in porous media supports a well-defined mode at wave vectors out to $Q = 3.6$ Å^{-1} at temperatures above the superfluid phase [6,12,14,16,17,19], i.e., at $T > T_C$, up to $T \simeq T_\lambda$. This has been interpreted as the existence of localized BEC (a Bose glass phase) at temperatures above T_C, i.e., in the temperature range $T_C < T < T_\lambda$. Localized BEC is pictured as puddles of BEC and superfluidity (but no extended BEC) in an otherwise normal liquid [7,8,12,17,19–21]. The puddles of BEC and superfluidity support well-defined P-R modes at higher wave vectors. The localized BEC "phase" lies between the superfluid and fully normal liquid phases. A recent direct measurement of both BEC and P-R modes in MCM-41 shows that the onset temperatures of BEC, $T_{\rm BEC}$, and of well-defined P-R modes, T_{PR}, at $Q > 0.8$ Å^{-1} coincide (i.e., $T_{PR} = T_{\rm BEC}$) [22].

The dynamic response of liquid ^{4}He in porous media also shows other features not found in bulk liquid ^{4}He. For example, the liquid layers nearest the pore walls support a layer mode [6,9–18,23]. The layer mode is observed at wave vectors in the roton region, 1.7 Å $< Q <$ 2.3 Å, only. The layer mode has a roton-like energy dispersion with Q at an energy lower than that of the roton. The layer mode energy gap in Vycor [12] is $\Delta_L = 0.55 \pm 0.01$ meV, significantly lower than the P-R mode roton energy gap, $\Delta = 0.742$ meV at

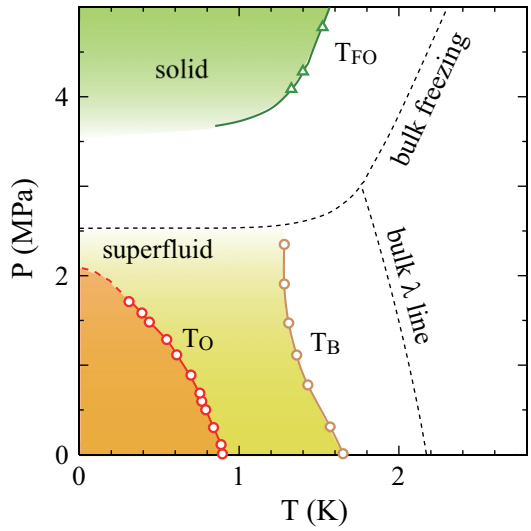

FIG. 1. Phase diagram of liquid ^{4}He in the present FSM-16 (from Ref. [21]). T_O is the onset temperature of superflow below which ρ_S/ρ has a temperature dependence similar to that in bulk liquid ^{4}He. T_B is the onset temperature of superflow in which ρ_S/ρ remains small. T_{FO} is the freezing temperature.

SVP. The specific heat arising from exciting this lower energy layer mode reproduces the specific heat of liquid ^{4}He in Vycor [9,12] and gelsil [8,17] well.

Much recent interest has turned to porous media consisting of arrays of straight nanopores that are not interconnected. Specific examples are FSM-16 (diameter $d = 28$ Å) [21,24–27] and MCM-41 ($d = 47$ Å) [20,22,28]. The distribution of pore diameters in the arrays is small (±3 Å) and the walls of the nanopores smoother [21] so that the confined ^{4}He may experience less disorder than in gelsil or Vycor. The initial ^{4}He that enters the pores is deposited in layers on the pore walls. This is the case for both the first solid layers and a few subsequent liquid layers. Simulation of ^{4}He in small-diameter nanopores [29–33] suggests that the liquid layers show 2D rather than 3D superfluid character. The line of liquid at the center of the nanopore can show 1D character [29–33]. There is an extensive literature on superfluidity, BEC, and modes in lower dimensional systems [34–37]. Our goal is to determine the P-R modes in FSM-16, particularly their temperature dependence, for comparison with some of these properties, particularly the superfluid properties.

Figure 1 shows the phase diagram of liquid ^{4}He in $d = 28$ Å FSM-16 reproduced from Ref. [21]. The temperature T_O identifies the onset of full superflow. T_O lies well below T_λ and T_O appears to go toward zero at higher pressure. T_B identifies the temperature at which a small fraction becomes superfluid at higher temperature. This fraction remains small at all temperatures until T_O is reached. T_B is identified as $T_{\rm BEC}$ in Ref. [21]. There is a solid phase in the pores at higher pressure, $p \gtrsim 36$ bars.

In this context, our aim is to determine the energy, width, and intensity in the P-R and layer modes in FSM-16 and their temperature dependence. Particularly, a goal is to determine T_{PR}, the onset temperature of well-defined P-R modes at $Q > 0.8$ Å^{-1} in the liquid. T_{PR} will be identified with the onset of BEC in FSM-16 nanopores as in other porous media. We investigate two pressures: (1) a pressure immediately below bulk SVP where there will be liquid in the FSM pores but no bulk liquid in the cell and (2) a pressure somewhat greater than the bulk solidification pressure ($p \geqslant 25.3$ bars at $T \to 0$ K) so that there will be solid ^{4}He everywhere in the cell except in the FSM-16 nanopores where there will be confined liquid under pressure. Two measurements of P-R modes in FSM at SVP have already been reported [18,38], an extensive measurement of modes at low temperature [18] and a measurement of the temperature dependence of the P-R mode [38] at the roton wave vector, $Q = 1.95$ Å^{-1}. We compare directly with these two measurements in the Discussion.

The paper is divided as follows. In Sec. II we describe the FSM-16 sample cell, the neutron scattering measurements, and the functions fitted to the data. The results are presented in Sec. III and discussed in Sec. IV.

II. EXPERIMENT

A. FSM-16 sample and sample cell

FSM-16 is an array of straight nanopores 28 Å in diameter arranged in a honeycomb structure of lattice constant 43.8 Å. The length of the nanopores is 0.2–0.5 μm and the sample is a powder of that grain size. The FSM-16 was kindly provided by Professor Junko Taniguchi. It is the same sample as used by Taniguchi *et al.* in measurements of the superfluid fraction [21,27], the specific heat [21], and other properties. The FSM-16 was synthesized by Inagaki *et al.* at Toyoto Central R&D Laboratories Inc., Japan. The FSM-16 sample size was 2.58 g in the measurement at SVP, 2.89 g in the measurement at 26 bars. The FSM-16 was held in a cylindrical aluminium sample cell of inner diameter 15 mm and height 69 mm. The top flange of the cell was copper to facilitate soldering to the filling tube. The sample and cell were outgassed at 150 °C and flushed with ^{4}He gas for a period of 24 hours. The cell was cooled using an ILL ^{3}He refrigerator in the measurement at SVP and using an ILL dilution refrigerator in that at 26 bars.

B. Neutron scattering measurements

The neutron scattering measurements of the dynamical structure factor (DSF), $S(Q, E)$, were conducted on the time-of-flight spectrometer IN5 at the Institut Laue-Langevin (ILL). The incident neutron wavelength was 4.8 Å and the IN5 energy resolution was 0.086 meV at zero energy transfer. The measurement procedure was the same as in previous measurements [14,15,20,39]. The data were analyzed using standard analysis packages such as LAMP at ILL.

C. Fitting functions

1. Model at SVP

The model DSF, $S(Q, E)$, that was fitted to the net observed scattering intensity from the ^{4}He in the cell observed at SVP was

$$S(Q, E) = S_{PR}(Q, E) + S_L(Q, E) + [n_B(E) + 1]S_B(Q, E). \quad (1)$$

$S_{PR}(Q,E)$ denotes the P-R mode and $S_L(Q,E)$ the layer mode observed at wave vectors in the roton region. $S_B(Q,E)$ is a broad background component. $S_B(Q,E)$ is obtained by a fit to data at low temperature and is held independent of temperature. It is multiplied by the Bose factor $[n_B(E)+1]$, where $n_B(E)=[\exp(E/k_BT)-1]^{-1}$ is the Bose function and k_B is Boltzmann's constant. The Bose function, $n_B(E)$, contributes at low energy only and higher temperature and is significant at wave vectors in the roton region only.

At SVP, $S_{PR}(Q,E)$ is represented by a damped harmonic oscillator (DHO) function,

$$S_D(Q,E) = \frac{Z_Q}{\pi}[n_B(E)+1]\left[\frac{\Gamma_Q}{(E-E_Q)^2+\Gamma_Q^2}-\frac{\Gamma_Q}{(E+E_Q)^2+\Gamma_Q^2}\right] = \frac{Z_Q}{\pi}[n_B(E)+1]\left[\frac{4EE_Q\Gamma_Q}{\left(E^2-\left[E_Q^2+\Gamma_Q^2\right]\right)^2+4E^2\Gamma_Q^2}\right], \quad (2)$$

where Z_Q, E_Q, and Γ_Q are the intensity, energy, and half-width of the mode. Z_Q, E_Q, and Γ_Q are treated as free fitting parameters as a function of temperature as discussed in the Results section. When the mode is sharply defined (Γ_Q is small compared to E_Q), Z_Q represents the intensity in the mode well. When Γ_Q is large, for example when the DHO is used to represent the broad scattering from the normal liquid, Z_Q becomes large and does not represent the intensity in a mode at all. The rationale for the DHO and the equivalence of the two expressions in Eq. (2) is given by Talbot *et al.* [40]. At SVP, the layer mode is also represented by a DHO where again Z_Q, E_Q, and Γ_Q are free fitting parameters.

2. Model at 26 bars

At 26 bars, where the scattering intensity is weak, we present data in the roton region only. Also at 26 bars the scattering from the normal liquid component, $S_N(Q,E)$, is significant. The normal component lies at an energy (near $E=0$) that is significantly lower than that of the roton and $S_N(Q,E)$ can be readily distinguished from the roton. The model fitted to the ^{4}He intensity is

$$S(Q,E)=S_R(Q,E)+S_N(Q,E), \quad (3)$$

where $S_R(Q,E)$ and $S_N(Q,E)$ are the roton mode and normal liquid components, respectively. At 26 bars, we represent $S_R(Q,E)$ by a Gaussian function,

$$S_G(Q,E)=Z_Q\left[\frac{1}{\left(2\pi\sigma_Q^2\right)^{1/2}}\right]\exp-\frac{(E-E_Q)^2}{2\sigma_Q^2}, \quad (4)$$

where Z_Q, E_Q, and σ_Q are free fitting parameters. In the fits of Eq. (4) to data, the intensity $Z_Q(T)$ in the Gaussian (the roton) decreases with increasing T. We represent the normal liquid $S_N(Q,E)$ by a DHO, Eq. (2). In fits to data, intensity $Z_Q(T)$ in the DHO increases with increasing T. The other parameters in the DHO and Gaussian were held independent of temperature.

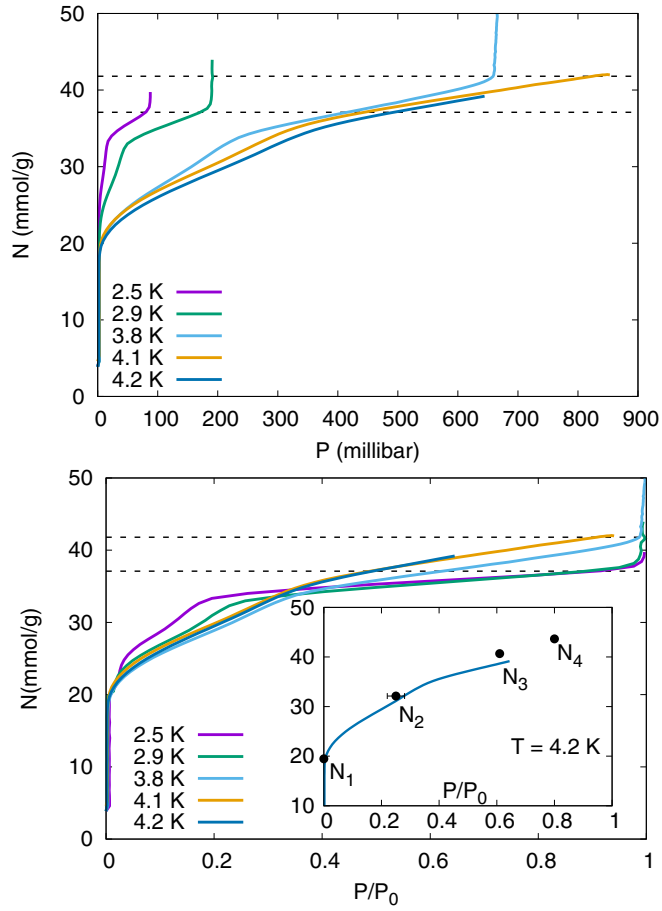

FIG. 2. Adsorption isotherms of ^{4}He in 28 Å pore diameter FSM-16 at several temperatures. N is the amount of ^{4}He added to the sample cell and P is the corresponding vapor pressure above the FSM. P_0 is the saturated vapor pressure (SVP) of bulk liquid ^{4}He. Completion of the tightly bound "dead" (solid) layers of ^{4}He on the FSM walls is taken as $N_S=22$ mmol/g. Full filling of the pores is taken as $N_{FF}=37$ mmol/g. Neutron scattering measurements were made at fillings $N_1=19.5$ mmol/g, $N_2=32$ mmol/g, $N_3=40.5$ mmol/g, and $N_4=43.5$ mmol/g (see inset).

III. RESULTS

A. Isotherms of ^{4}He in FSM-16

Figure 2 shows absorption isotherms of ^{4}He in the present FSM sample at several temperatures. Shown is the amount, N, of ^{4}He added to the cell, in units of mmol of helium per gram of FSM in the cell, versus the vapor pressure, P, above the FSM. P is in units of mbar in the upper panel and in units of the saturated vapor pressure (SVP) of bulk liquid ^{4}He, P_0, in the lower panel. The initial ^{4}He going into the cell forms layers of ^{4}He tightly bound to the FSM nanopore walls, often denoted "dead" layers. The vapor pressure, P, above these tightly bound "dead" layers is small. In Fig. 2, the pressure P remains very small up to a filling of $N=20$–24 mmol/g and rises thereafter. We take $N_S=22$ mmol/g as completion of the "dead" layers in the present sample.

The subsequent layers are less tightly bound liquid and P increases. In a pore of diameter $d=28$ Å (radius $R=14$ Å) if the filling were in uniform layers, the pore would be full

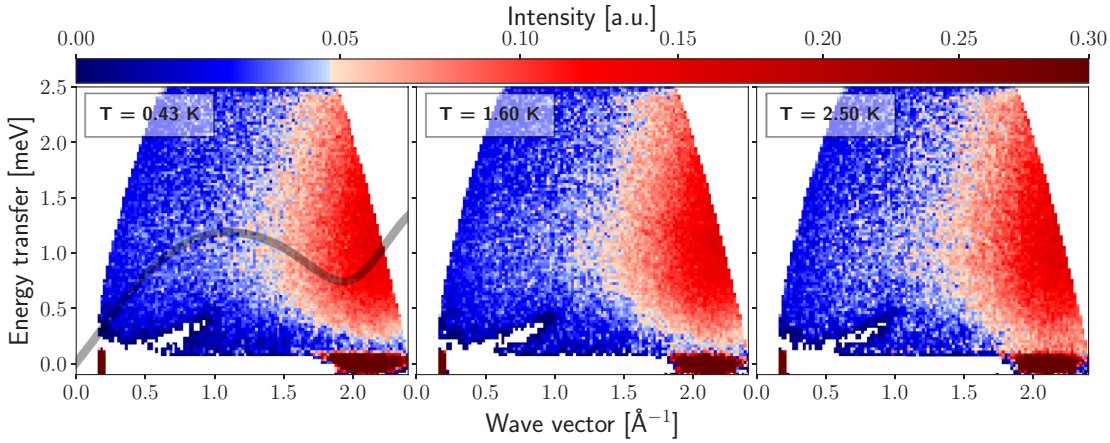

FIG. 3. Net scattering intensity, $S(Q, E)$, from ^{4}He in the sample cell at filling (1), $N_1 = 19.5$ mmol/g; "dead" (solid) layers of ^{4}He on the pore walls only. Q is the wave vector transfer and E is the energy transfer. The solid line is the P-R mode energy dispersion curve in bulk liquid ^{4}He at low temperature from Ref. [42] shown to set the energy scale. Three temperatures are shown, $T = 0.43$ K, 1.6 K, and 2.5 K. Broad, temperature-independent scattering from the "dead" layers is observed.

after the "dead" layers and 3 additional liquid layers with the maximum density of the third liquid layer lying at the center of the pore [32]. In FSM-16, however, the filling of the liquid layers does not appear to be uniform along the pore. Rather, some regions are fully filled at low fillings while other regions have liquid films (see Sec. IV A).

When P reaches P_0, the SVP of bulk liquid ^{4}He, the FSM is full. Any further ^{4}He added goes into bulk liquid around the FSM at a constant pressure P_0. In Fig. 2 full filling can be identified as a vertical rise in N at constant $P = P_0$. At $T = 2.5$ K, P_0 is low (85 mbar) and at full filling essentially all the ^{4}He added to the cell has gone into the FSM-16 with little ^{4}He in the vapor in the cell above the FSM-16. From the isotherm at 2.5 K in Fig. 2, we take full filling at $N_{FF} = 37$ mmol/g. In contrast, at $T = 3.8$ K, the SVP, P_0, is significant (660 mbar). At 3.8 K the apparent full filling in Fig. 2 (the vertical rise in N) is at $N \simeq 42$ mmol/g added to the cell. However, there is still just 37 mmol/g in the FSM-16 and roughly 5 mmol/g has gone into the ^{4}He vapor outside the FSM pores at pressure $P_0 = 660$ mbar.

In small-pore media such as 25 Å and 44 Å MPD gelsil, P-R modes are observed at fillings almost immediately after the filling of the "dead" layers is complete [14,15]. In larger pore media such as aerogel [12], further filling corresponding to another liquid layer is needed before modes are observed. In gelsils, there is a broad distribution of pore volumes [16] and smaller volumes fill first. On a wide variety of surfaces, a threshold coverage [41] of $n_0 = 26\mu$mol/m^2 is needed before superfluidity is observed. Using 1173 m^2/g for the present FSM sample [61], this threshold corresponds to a filling $N_0 = 30.5$ mmol/g. We have observed modes at lower fillings in FSM-16, e.g., 28 mmol/g, and superfluidity has similarly been observed below 30 mmol/g. This suggests again that there is nonuniform filling along the FSM pores with some regions of the pores full at fillings well below completely full pores, $N_{FF} = 37$ mmol/g.

We present neutron scattering results at four fillings: (1) $N_1 = 19.5$ mmol/g, (2) $N_2 = 32$ mmol/g, (3) $N_3 = 40.5$ mmol/g, and (4) $N_4 = 43.5$ mmol/g as shown in Fig. 2. The scattering from ^{4}He taken at these fillings will represent scattering (1) from "dead" (solid) ^{4}He layers on the nanopore walls, (2) from solid layers plus liquid including superfluid liquid in the FSM-16 at a filling fraction $f = N_2/N_{FF} = 32/37 = 86\%$, and (3) and (4) from fully filled FSM plus bulk liquid ^{4}He outside the FSM.

B. Filling dependence of $S(Q, E)$

In this section we present maps of the scattering intensity, proportional to the dynamic structure factor, $S(Q, E)$, observed in the neutron scattering measurements at fillings N_1 to N_4 as a function of temperature. The fillings, N_1 to N_4, are shown in an inset in Fig. 2. We subsequently present data taken at 26 bars, which are necessarily taken at full filling of the FSM-16.

Figure 3 shows an intensity map of the observed $S(Q, E)$ versus Q and energy transfer, E, at filling $N_1 = 19.5$ mmol/g. Since $N_1 \lesssim N_S$ there are only "dead" (solid) layers of ^{4}He on the pore walls. $S(Q, E)$ arising from the solid layers has no well-defined modes. It is a broad function of Q and E that has a maximum at $Q \geqslant 2$ Å^{-1} and $E \simeq 1$ meV. $S(Q, E)$ also has little temperature dependence up to 2.5 K. The gray line is the P-R mode dispersion curve in bulk liquid ^{4}He at $T \to 0$ K shown to set the scale [42].

Figure 4 shows the observed $S(Q, E)$ at filling $N_2 = 32$ mmol/g, "dead" layers on the walls plus liquid within the FSM nanopores. A P-R mode in the confined liquid is observed. The mode has a width at low temperature and broadens further with increasing temperature. The mode is most intense at wave vectors in the roton region $1.7 \leqslant Q \leqslant 2.3$ Å^{-1} as in the bulk liquid [43]. No P-R mode is observed at temperatures 1.8 K and 2.0 K.

Figure 5 shows $S(Q, E)$ at filling $N_4 = 43.5$ mmol/g. Since the FSM-16 is full at $N_{FF} = 37$ mmol/g, there is roughly 7 mmol/g of bulk liquid in the cell at N_4. An intense P-R mode is observed at lower temperatures characteristic of bulk liquid ^{4}He. The mode broadens with increasing temperature and no

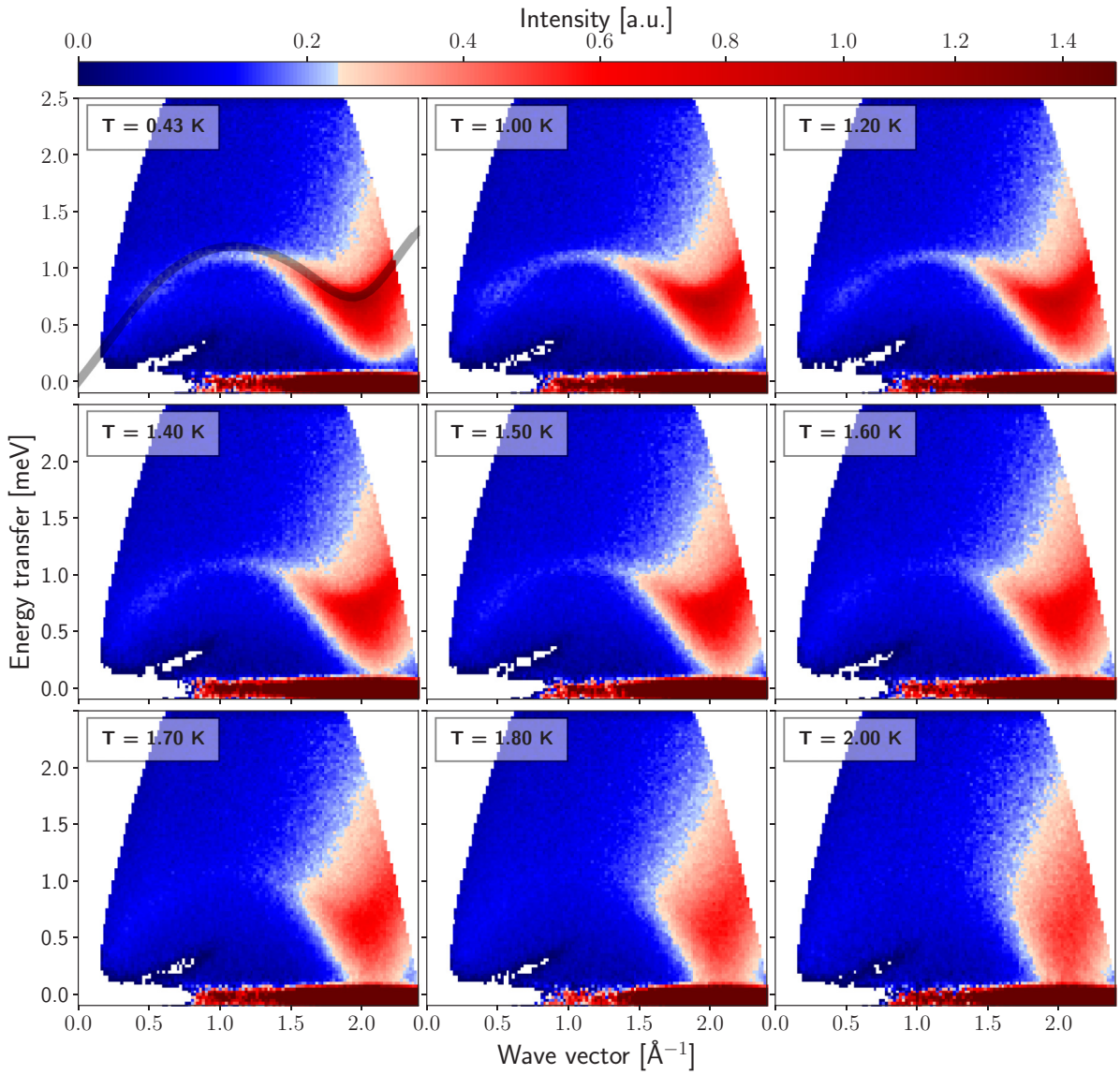

FIG. 4. As Fig. 3 at filling (2), $N_2 = 32$ mmol/g; "dead" layers plus liquid in the nanopores (full pores at $N_{FF} = 37$ mmol/g). Nine temperatures are shown. A P-R mode in the liquid in the pores is observed at temperatures less than $T = 1.8$ K.

mode is observed in the roton region, $Q \simeq 2$ Å^{-1}, at 2.2 K or 2.5 K where bulk normal liquid (no BEC) is anticipated. However, a mode in the phonon region, $Q \leqslant 0.8$ Å^{-1}, is observed in the bulk normal liquid up to 2.2 K.

Figure 6 shows the net $S(Q, E)$ from the ^{4}He in FSM-16 at four fillings at the specific wave vectors $Q = 1.1$ Å^{-1} and 1.95 Å^{-1}. There is a large elastic scattering peak at $E = 0$. At filling (1), $N_1 = 19.5$ mmol/g, there is broad inelastic scattering from the solid layers on the pore walls at both wave vectors. At filling (2), $N_2 = 32$ mmol/g, and $Q = 1.1$ Å^{-1} there is a mode of modest intensity observed at $E = 1.1$ meV. At fillings (3) and (4) there is a large, well-defined peak at $Q = 1.1$ Å^{-1} arising from the P-R mode in the bulk liquid in the cell. At $Q = 1.1$ Å^{-1} there is also a broad peak centered at $E = 0.75$ meV arising from the roton seen at $Q = 1.1$ Å^{-1} via multiple helium-FSM scattering. A similar $S(Q, E)$ is observed at $Q = 1.95$ Å^{-1}. Clearly, the scattering intensity from the P-R modes in the liquid confined in the FSM is much weaker than that from the bulk liquid.

C. Phonon-roton energy dispersion curve at 0.43 K

Figure 7 shows the P-R mode energy dispersion curve of liquid ^{4}He in FSM at filling 32 mmol/g and in bulk liquid ^{4}He at low temperature. The curve extends out to $Q = 2.4$ Å^{-1}, the maximum Q accessible on IN5. At low Q, the phonon energies and the sound velocity are the same in FSM and bulk within precision. At the wave vectors in the region $Q \simeq 1.1$ Å^{-1}, the energies in FSM lie below those in the bulk liquid. For example, at $Q = 1.1$ Å^{-1}, the P-R mode energy in FSM is $E_Q = 1.11(2)$ meV compared with $E_Q = 1.18(3)$ meV in the bulk liquid [44]. An E_Q below the bulk value at wave vectors $Q \simeq 1.1$ Å is widely observed in films of ^{4}He on flat surfaces [45] and on surfaces in porous media [11,12,15]. In the roton

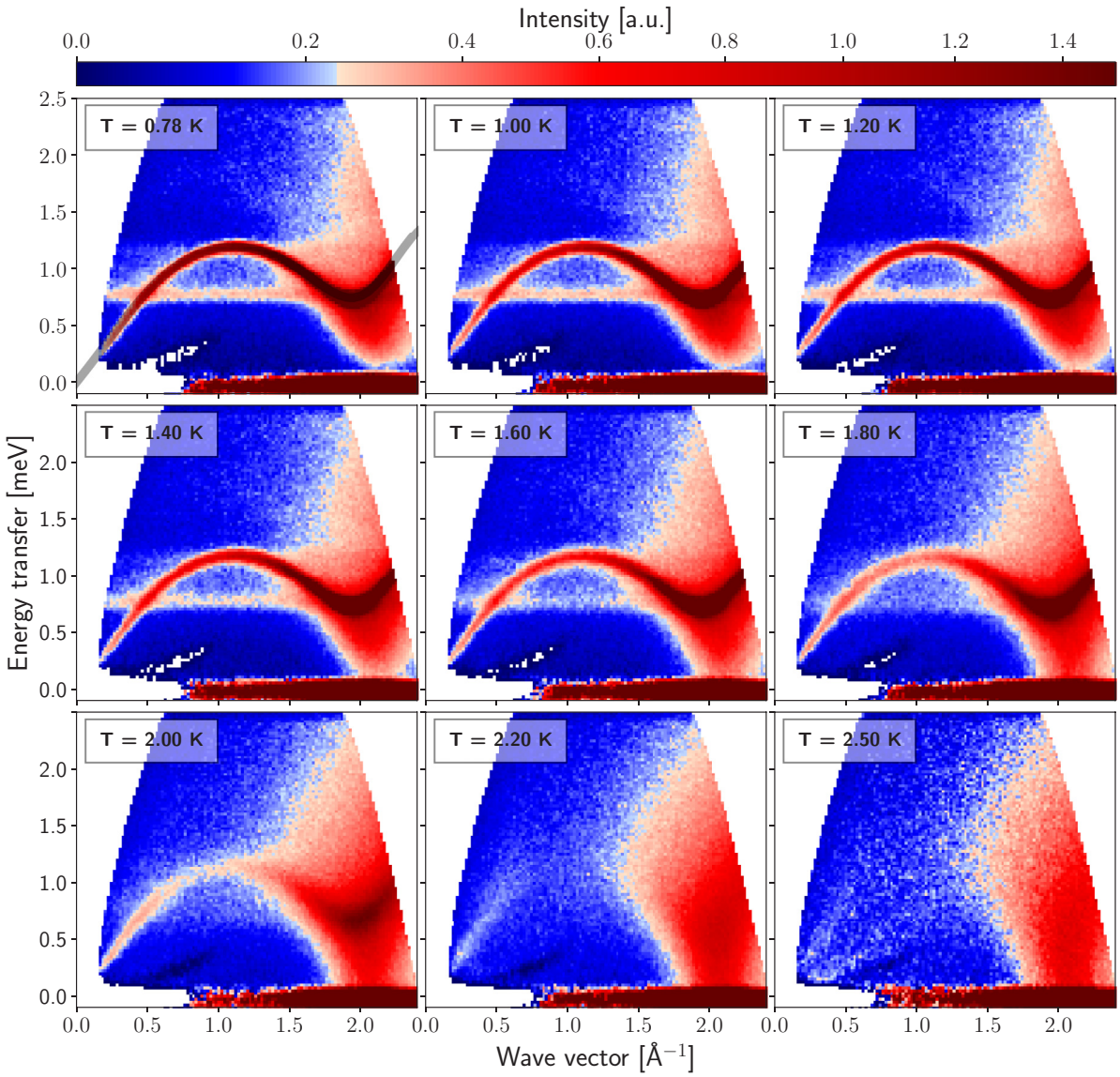

FIG. 5. As Fig. 3 at filling (4), $N_4 = 43.5$ mmol/g, overfilled nanopores. An intense, well-defined P-R mode of bulk liquid ^{4}He and multiple scattering from the roton at temperatures up to $T = 2.0$ K is observed.

region, $Q \simeq 1.95$ Å^{-1}, the mode energies in FSM are again the same as those in bulk liquid ^{4}He within precision.

D. Temperature dependence of $S(Q, E)$ at SVP

The temperature dependence of $S(Q, E)$ of liquid ^{4}He in FSM-16 at filling (2), $N_2 = 32$ mmol/g, is shown in Fig. 8 at $Q = 1.1$ Å^{-1} and 1.95 Å^{-1}. The aim is to determine the temperature, T_{PR}, at which well-defined modes are no longer observed directly from the data. As temperature is increased, the P-R mode broadens and the intensity in the mode decreases, particularly at $T \geqslant 1.2$ K. At $Q = 1.1$ Å^{-1}, the mode is observed up to but not above 1.7 K. At 1.8 K and 2.0 K there is no mode at $Q = 1.1$ Å^{-1}. $S(Q, E)$ changes little with temperature between 1.8 K and 2.0 K. Similarly, at the roton wave vector, $Q = 1.95$ Å^{-1}, the P-R mode broadens and decreases in intensity with increasing temperature. The temperature at which the P-R mode is last observed is more difficult to identify precisely at $Q = 1.95$ Å^{-1} since $S(Q, E)$ continues to change with increasing temperature above 1.8 K. From the data at $Q = 1.1$ Å^{-1} we take $T_{PR} = 1.8$ K at SVP. We identify T_{PR} with T_{BEC}, the onset temperature of BEC.

E. Fits to the temperature dependence of $S(Q, E)$ at SVP

To confirm the temperature at which the P-R mode is last observed, T_{PR}, and to determine P-R mode energies and widths, we fit the model given by Eqs. (1) and (2) to the net $S(Q, E)$ of ^{4}He in FSM-16 at filling $N_2 = 32$ mmol/g at $Q = 1.1$ Å^{-1} and $Q = 1.95$ Å^{-1}.

1. $Q = 1.1$ Å^{-1}

At $Q = 1.1$ Å^{-1} there is no layer mode. Equation (1) is therefore modified to consist of a DHO fitted to the P-R

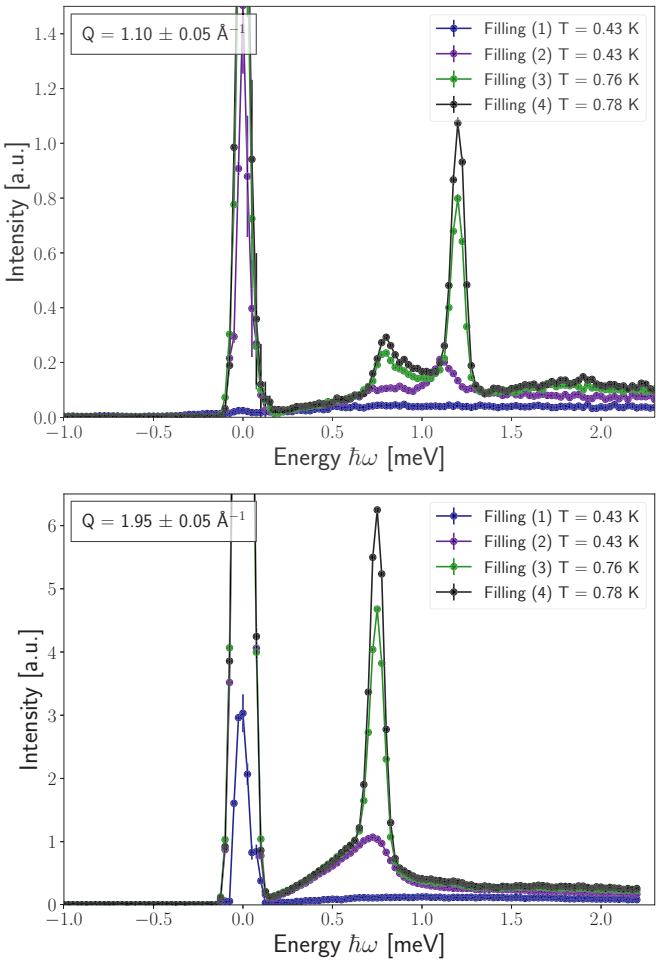

FIG. 6. Net scattering intensity from ^{4}He in the sample cell at four fillings: upper panel, $Q = 1.1$ Å^{-1}, and lower panel, $Q = 1.95$ Å^{-1}. The large peak at $E = 0$ is elastic scattering from the ^{4}He. At filling (1), "dead" layers of solid ^{4}He on the pore walls only; broad inelastic intensity is observed. At filling (2), "dead" layers plus liquid ^{4}He in the pores; a P-R mode in the confined liquid is observed at $E = 1.10(2)$ meV ($Q = 1.1$ Å^{-1}) and at $E = 0.742(2)$ meV ($Q = 1.95$ Å^{-1}). At fillings (3) and (4), where the FSM-16 is overfilled, scattering from the P-R mode in the bulk liquid ^{4}He outside the pores dominates. The weaker peak at $E \simeq 0.75$ meV at $Q = 1.1$ Å^{-1} is the roton observed at $Q = 1.1$ Å^{-1} via multiple scattering.

mode at $E = 1.1$ meV and a second DHO fitted to the roton mode at $E = 0.75$ meV observed at $Q = 1.1$ Å^{-1} via multiple scattering and a background function, $S_B(Q, E)$, that is held independent of temperature. $S_B(Q, E)$ arises chiefly from the "dead" layers tightly bound to the nanopore walls. The model is convoluted with the instrument resolution of IN5 before the fit to data. We present best-fit values of E_Q, $2\Gamma_Q$, and Z_Q for the P-R mode only.

We consider two choices for the background function, $S_B(Q, E)$. In the first, $S_B(Q, E)$ is determined by a fit to the broad scattering at $T = 1.8$ K where there is no P-R mode peak. $S_B(Q, E)$ is subtracted from $S(Q, E)$ and the two DHOs are fitted to the remaining intensity. The fit to data and the best-fit values of E_Q, $2\Gamma_Q$, and Z_Q for the P-R mode are shown in the two panels on the left-hand side of Fig. 9 as

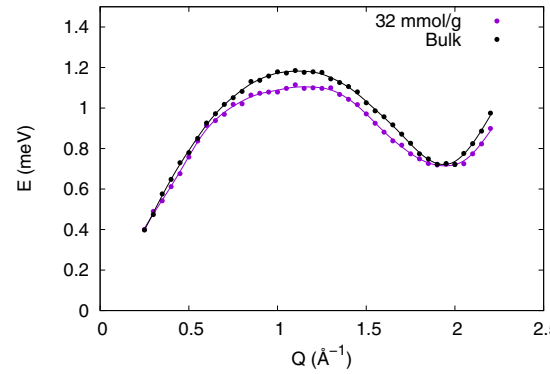

FIG. 7. Phonon-roton mode energy dispersion curve, E_Q vs Q, of liquid ^{4}He in FSM-16 at filling $N_2 = 32$ mmol/g and in bulk liquid at $T = 0.43$ K and 0.78 K, respectively. At wave vector transfers $Q \simeq 1.1$ Å^{-1} the E_Q of liquid ^{4}He in FSM-16 lies below the bulk liquid E_Q.

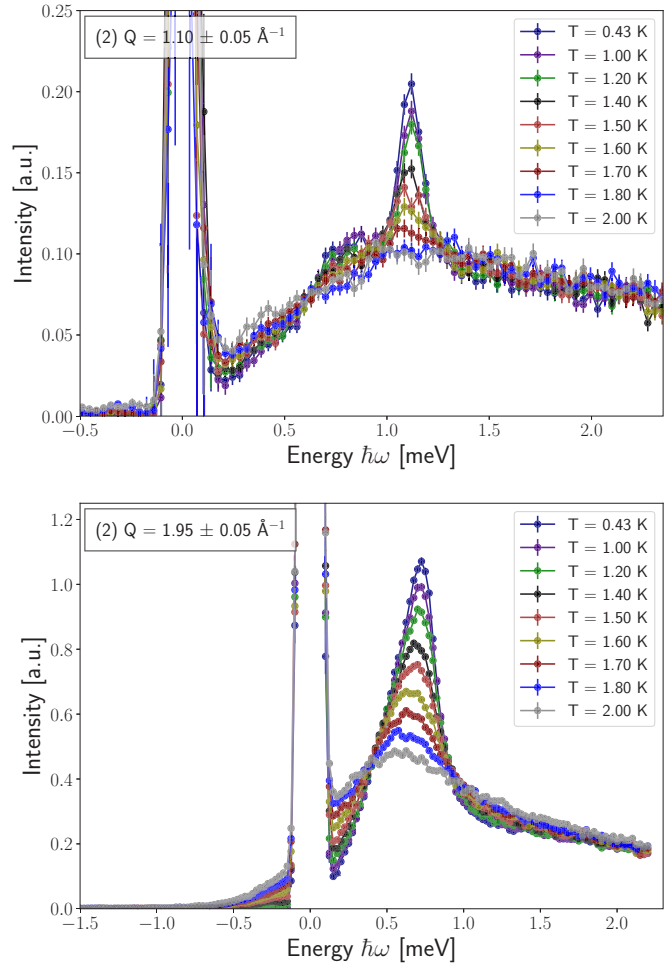

FIG. 8. Net scattering intensity from ^{4}He in FSM-16 vs temperature at filling (2), $N_2 = 32$ mmol/g ("dead" layers and liquid in the pores), at wave vector transfer $Q = 1.1$ Å^{-1} (upper panel) and $Q = 1.95$ Å^{-1} (lower panel). At $Q = 1.1$ Å^{-1} the P-R mode is observed at 1.10(2) meV and at $Q = 1.95$ Å^{-1} at 0.742(2) meV. The large peak centered at $E = 0$ is elastic scattering.

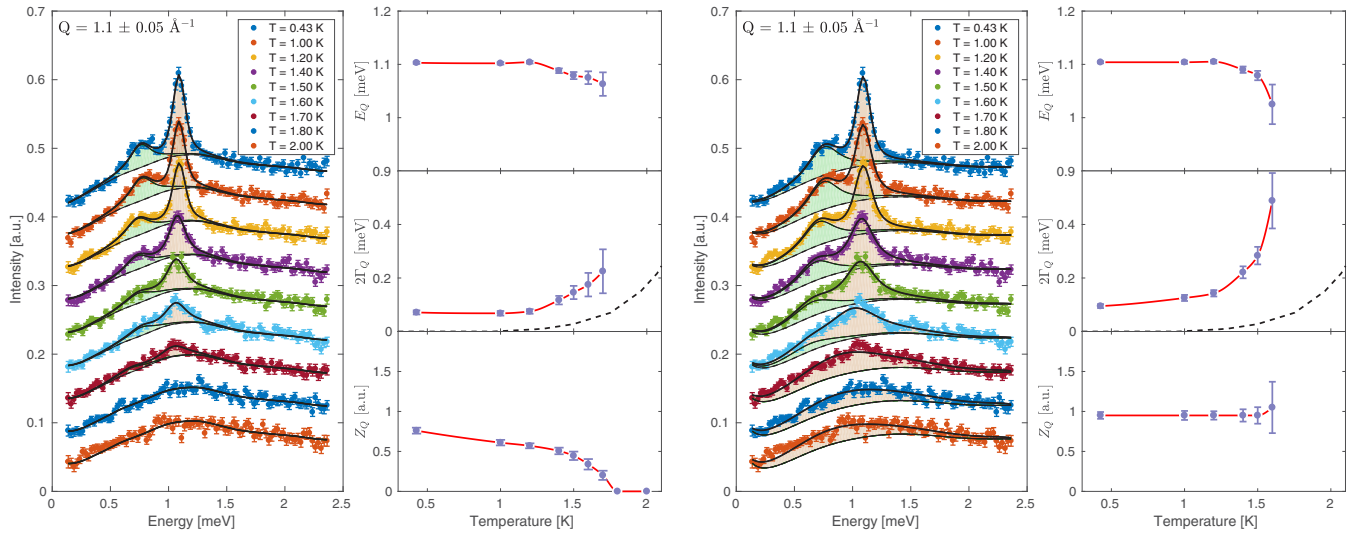

FIG. 9. The net scattering intensity, $S(Q, E)$, at filling (2) and $Q = 1.1$ Å^{-1} with a fit to data vs temperature. Shown are the data (as in Fig. 8) (data points), the fit to $S(Q, E)$ (black line fitted to data points), and the best-fit parameters, E_Q, $2\Gamma_Q$, and Z_Q, in the DHO, Eq. (2), fitted to the P-R mode. In the left two panels the background function, $S_B(Q, E)$, in $S(Q, E)$ of Eq. (1), was chosen to fit the broad intensity observed at $T = 1.8$ K where there are no modes. In the right two panels $S_B(Q, E)$ was chosen to fit the broad intensity observed at $T = 0.43$ K.

a function of temperature. The mode energy, E_Q, remains roughly independent of temperature up to 1.2 K and then decreases with increasing temperature. The width, $2\Gamma_Q$, is large at low temperature, roughly five times the bulk liquid value at 1.4 K. The intensity, Z_Q, in the mode goes to zero at $T = 1.8$ K. The errors in the fit parameters are small at low temperature but are larger at high temperature because the intensity in the P-R mode is small at high temperature.

In the second choice, the background function, $S_B(Q, E)$, is determined by a fit to the uniform intensity observed at $T = 0.45$ K, the lowest measured temperature. $S_B(Q, E)$ is again subtracted from $S(Q, E)$ and the two DHOs fitted to the remaining intensity. The fit to data and the best-fit values of E_Q, $2\Gamma_Q$, and Z_Q are shown in the two panels on the right-hand side of Fig. 9. The best-fit value of E_Q is again roughly independent of temperature up to 1.2 K. The width is again large at low temperature and $2\Gamma_Q$ increases dramatically at higher temperature. Z_Q is essentially constant, independent of T up to 1.6 K.

The two fits find the same mode energy and a large width at low temperature. In both fits there is no mode, only broad response, at $T = 1.8$ K. However, in the first fit, the parameter Z_Q goes to zero at 1.8 K and $2\Gamma_Q$ increases somewhat with temperature. In contrast, in the second fit, Z_Q remains constant at higher temperature and $2\Gamma_Q$ increases markedly as $T \rightarrow 1.8$ K.

This difference can be understood from the choice of $S_B(Q, E)$ and the nature of the DHO. Consider the first DHO expression for $S_{PR}(Q, E)$ in Eq. (2). For energies, E, near the P-R mode peak, $E \simeq E_Q$, and a significant width, Γ_Q, i.e., $(E - E_Q) \ll \Gamma_Q$, the expression for $S_{PR}(Q, E)$ reduces to $S(Q, E \simeq E_Q) = Z_Q/\pi\Gamma_Q$ [$n(E_Q)$ is negligible]. At higher temperature a small P-R mode peak height can therefore be obtained if (1) $Z_Q \rightarrow 0$ or (2) Γ_Q becomes large. Whether it is (1) or (2) depends on how $S_B(Q, E)$ is chosen.

If $S_B(Q, E)$ is chosen as the broad intensity at $T = 1.8$ K and this is subtracted from $S(Q, E)$, the remaining P-R mode intensity will show a significant well-defined peak at low temperature. However, when temperature is increased and returned to 1.8 K, the intensity in $S_{PR}(Q, E)$ must go to zero. This will be described in a fit by having Z_Q be zero at 1.8 K. If $S_B(Q, E)$ is chosen as the broad intensity at 0.45 K, the remaining P-R mode intensity will again show the same significant peak at low temperature. As temperature is increased, the mode broadens and loses intensity but the intensity that was in the peak at low temperature must remain in $S(Q, E)$ at higher temperature. The fit will describe this broadened intensity at higher temperature by having Γ_Q become large. The data and fit give the same result, no peak at higher temperature $T = T_{PR} = 1.8$ K, but the mode parameters are quite different at higher temperature. These fits correspond to a simplified Woods-Svensson (WS) and a simple subtraction (SS) fit, respectively [40,43,44,46,47].

2. $Q = 1.95$ Å^{-1}

We now fit the model Eq. (1) to the net $S(Q, E)$ of ^{4}He in FSM-16 observed at $Q = 1.95$ Å^{-1}. The aim is to determine the energy, width, and intensity of the P-R and layer modes of the confined liquid as a function of temperature. In Eq. (1), $S_{PR}(Q, E)$ represents the P-R mode, $S_L(Q, E)$ the layer mode, and $S_B(Q, E)$ the "background" intensity outside the modes. $S_B(Q, E)$ is determined by a fit to the uniform broad intensity observed at $T = 0.45$ K.

In the fit, $S_B(Q, E)$ is held independent of temperature and subtracted from the data at each temperature. $S_{PR}(Q, E) + S_L(Q, E)$ is fitted to the remaining $S(Q, E)$ as a function of temperature. This corresponds to a simple subtraction (SS) method [40,44,48] in which the background component is simply subtracted from the total $S(Q, E)$. In Eq. (1) $S_B(Q, E)$

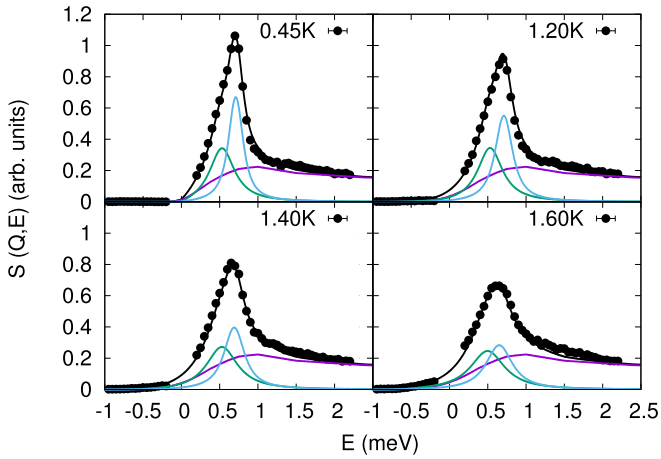

FIG. 10. Net scattering intensity, $S(Q, E)$, at filling (2) and $Q = 1.95$ Å^{-1} (data points) with a fit of Eq. (1) at four temperatures. The background function $S_B(Q, E)$ in Eq. (1) is determined by a fit to the broad intensity observed at $T = 0.43$ K. A damped harmonic oscillator (DHO), Eq. (2), is fitted to both the P-R mode (peaked at $E = 0.742(2)$ meV) and the layer mode (peaked at $E = 0.53$ meV). The width of both the P-R and layer modes increases with increasing temperature.

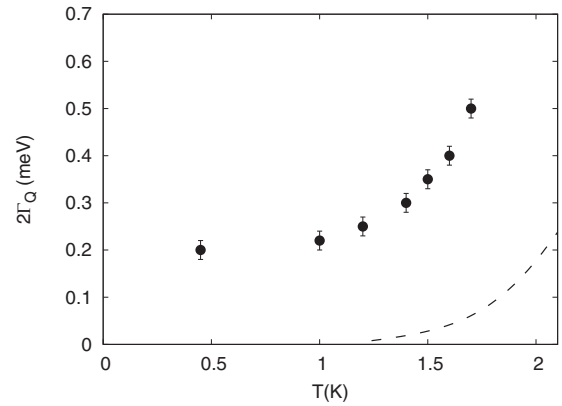

FIG. 11. The roton mode width, $2\Gamma_Q$, at the roton wave vector, $Q = 1.95$ Å^{-1} (data points), obtained from the fit of a DHO, Eq. (2), to the roton mode shown in Fig. 10. In the fit the parameters E_Q and Z_Q in the DHO changed little with temperature up to 1.6 K. Dashed line is $2\Gamma_Q$ in bulk liquid ^{4}He.

is multiplied by a Bose factor, significant only at higher temperatures and low energy, $E \lesssim 0.3$ meV. $S_{PR}(Q, E)$ and $S_L(Q, E)$ are both represented by DHO functions, Eq. (2).

Figure 10 shows the fit of Eq. (1) to the net intensity at $Q = 1.95$ Å^{-1} at four temperatures up to $T = 1.6$ K. The E_Q, Γ_Q, and Z_Q in the DHO describing both the P-R and layer modes were treated as free fitting parameters as a function temperature. In Fig. 10, we see that the model provides a good fit to data up to $T = 1.6$ K. Above 1.6 K, a normal liquid component is needed to provide a good fit to data. At $T = 0.45$ K, the best-fit roton energy, E_Q, agrees well with the bulk liquid roton energy, $\Delta = 0.742$ meV. The roton energy, E_Q, was independent of temperature up to 1.2 K and then decreased at higher temperatures as found [43,44,49,50] in bulk liquid ^{4}He. The width, Γ_Q, is shown as a function of temperature in Fig. 11. The width is large at $T = 0.45$ K and increases substantially at higher temperature, as found above at $Q = 1.1$ Å^{-1} and shown on the right-hand side of Fig. 9. If the background, $S_B(Q, E)$, had been chosen by a fit to data in the normal phase, the width would be the same at $T = 0.45$ K with a somewhat smaller increase in width with temperature, as shown on the left-hand side of Fig. 9 at $Q = 1.1$ Å^{-1}. The roton width of liquid ^{4}He in FSM-16 is clearly significantly larger than that in bulk liquid ^{4}He, e.g., at 1.4 K, 15 times larger than the bulk value, as discussed in Sec. IV C.

In the fits, Z_Q was found to be independent of temperature up to 1.6 K. In bulk liquid ^{4}He Z_Q is independent of temperature up to 1.8 K in the SS model [40,43,44,49]. Z_Q is constant in the SS model because the static structure factor, $S(Q)$, is independent of temperature (within 5 %). That is, since $S_B(Q, E)$ is held independent of temperature, the corresponding $S_B(Q)$ will be independent of temperature. The remaining $S_{PR}(Q)$ arising from the P-R mode, after $S_B(Q)$ is subtracted from a constant $S(Q)$, must also be independent of temperature. Since $S_{PR}(Q) = Z_Q[\frac{2}{\pi}\tan^{-1}(\frac{E_Q}{\Gamma_Q})] \simeq Z_Q$, the Z_Q must be approximately constant. Indeed in bulk liquid ^{4}He, the fitted Z_Q increases very slightly with temperature as Γ_Q increases to keep $S_{PR}(Q)$ constant (e.g., see Fig. 8 of Ref. [40]). In the roton case in FSM, $S_L(Q, E)$ was also largely independent of temperature up to 1.6 K. Thus we anticipate a Z_Q that is approximately independent of temperature in the above SS fit to data in FSM-16.

The layer mode is broad at low temperature. It may consist of more than one mode. A DHO centered at $\Delta_L = 0.53 \pm 0.03$ meV with FWHM $= 0.40$ meV provides a good fit at $T = 0.45$ K. The layer mode is robust and well defined up to 1.6 K as shown in Fig. 10. There is some reduction of the mode intensity at higher temperatures $T > 1.5$ K. However, it becomes difficult to distinguish the layer mode from a possible normal liquid component in $S(Q, E)$ at $T > 1.5$ K. The layer mode may survive into the normal phase, i.e., to temperatures $T > T_{PR} = T_{\rm BEC} = 1.8$ K. The Δ_L measured with neutrons agrees well with the Δ_L extracted from the specific heat of FSM-16 as discussed below in Sec. IV C. The layer mode energy observed [11,12] using neutrons in Vycor and aerogel is 0.55 ± 0.01 meV and 0.63 ± 0.01 meV, respectively. The broadening of both the roton and the layer modes with increasing temperature is clearly visible in Fig. 10.

F. Temperature dependence of $S(Q, E)$ at 26 bars

The sound velocity and phonon mode energies increase with increasing pressure. In contrast the mode energy at the roton minimum, Δ, decreases with increasing pressure, to $\Delta = 0.62$ meV at 26 bars. A well-defined P-R mode is observed only if the mode energy, E_Q, is less than twice the roton energy, 2Δ. If E_Q exceeds 2Δ, the mode can decay spontaneously to two rotons and only broad response is observed. For this reason, at 26 bars a well-defined P-R mode may not be observed or may be broadened [39] at wave vectors near the "maxon" wave vector $Q = 1.1$ Å^{-1}. To observe well-defined modes at 26 bars, we focused on wave vectors in the roton region only.

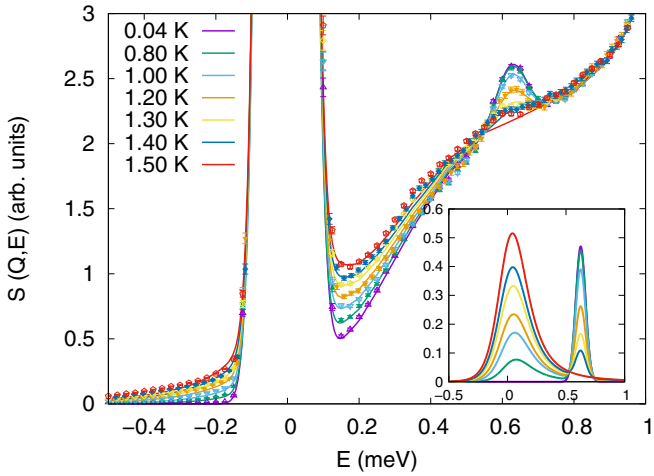

FIG. 12. Scattering intensity observed from ^{4}He in and around FSM-16 at pressure 26 bars at the roton wave vector, $Q = 2.10\,\text{Å}^{-1}$, and several temperatures. The large peak at $E = 0$ is elastic scattering. The large, temperature-independent sloping background is inelastic scattering from phonons in the solid ^{4}He around the FSM. The temperature-dependent inelastic scattering is interpreted as scattering from the roton and the normal liquid in the FSM-16. The small peak at $E = 0.62$ meV is the roton. The inset shows the temperature dependence of a fit of a DHO, Eq. (2), to the normal liquid component (peaked near $E \simeq 0$) and a Gaussian, Eq. (4), to the roton. The intensity in the roton peak is zero at $T = 1.5$ K.

The scattering intensity at 26 bars at the roton wave vector $Q = 2.1\,\text{Å}^{-1}$ is shown in Fig. 12 as a function of temperature. The large peak at $E = 0$ is elastic scattering. The peak centered at 0.62 meV on a sloping background is the roton. The inelastic sloping background arises from scattering from the phonons in the solid ^{4}He around the FSM-16. This background was assumed to be independent of temperature (up to 1.5 K) and was subtracted from the total scattering intensity to obtain the net scattering from the liquid in the pores. The roton is observed at low temperature but has disappeared at $T = 1.5$ K, i.e., $T_{PR} = 1.5$ K. We identify the maximum temperature at which BEC exists in the liquid as the temperature T_{PR} at which P-R modes are no longer observed, i.e., $T_{\text{BEC}} = T_{PR} = 1.5$ K at 26 bars.

The inset in Fig. 12 shows a model fitted to the scattering intensity arising from the liquid as a function of temperature. The model consists of a Gaussian function centered at $E = 0.62$ meV that represents the roton and a DHO that peaks at $E \simeq 0.1$ meV that represents the normal liquid component. The Gaussian has a width at $T = 0.45$ K of 0.12 meV that is held independent of temperature. The width may increase with increasing temperature. However, since there is already a substantial width at $T = 0.45$ K and the mode can be fitted up to $T \simeq 1.4$ K only, we were not able to identify any increase. The intensity in the Gaussian decreases with increasing temperature. The normal liquid component peaks at a much lower energy at 26 bars than it does at SVP and can be readily separated from roton intensity. As observed in the bulk liquid ^{4}He and in liquid ^{4}He in other porous media, the peak of the normal liquid response moves to lower energy with increasing pressure as the liquid becomes more classical (see Fig. 18 of Ref. [43]). At 26 bars the peak is close to $E = 0$. A layer mode was not identified in FSM-16 at 26 bars.

The intensity in the roton mode decreases with increasing temperature and that in the normal liquid component increases until the normal liquid component contains all the intensity at $T = 1.5$ K. An interesting feature is that as temperature is increased, the increase in the intensity in the normal liquid component, $S_N(Q, E)$, is greater than the loss of the intensity in the roton mode, $S_R(Q, E)$. This is consistent with some melting of the solid layers to normal liquid as T is increased so that there is more liquid in the pores at higher temperature.

IV. DISCUSSION

A. Filling dependence

On flat surfaces and on the surfaces of large-pore media, such as aerogel and Vycor, ^{4}He is deposited in layers. The initial layers are tightly bound to the surface and denoted "dead" layers. Data in a range of silica-based porous media are consistent with 1.5 "dead" layers 5 Å thick [2,24]. The "dead" layers are believed to be predominantly solid but may contain some tightly bound liquid. This is followed by liquid layers. Measurements of the static structure factor, $S(Q)$, in aerogel [51] and 34 Å mean pore diameter (MPD) gelsil [16] indicate that the "dead" layers are an amorphous solid that has the same density as the subsequent liquid layers. In large-pore media, modes in the liquid are first observed only in the second and subsequent liquid layers [11,12]. Superfluidity begins at a higher coverage of $n_0 = 26\ \mu\text{mol/m}^2$ on a variety of substrates [41]. At coverages below n_0, the liquid at low temperature is interpreted as a non-superfluid liquid localized by interaction with the substrate [2,41].

The "dead" layers, which are dominated by interaction with the surface, appear to be the same in small and large pore media. Indeed, in MCM-41 of pore diameter 32 Å, the "dead" layers are complete at 60% filling of the pores [28]. In the present FSM-16, the "dead" layers are complete at a filling of $N_S = 22$ mmol/g. With full filling at $N_{FF} = 37$ mmol/g this similarly gives "dead" layers complete at a filling of 60%. Assuming a "dead" layer density the same as the subsequent liquid layers and cylindrical pores, we obtain a "dead" layer thickness of 5.1 Å in FSM-16, consistent with that in larger pore media.

However, beyond the "dead" layers the filling appears to be quite different and nonuniform in small-pore media. In 25 Å MPD geltech [14] and 44 Å MPD gelsil [15], both P-R and layer modes are first observed at fillings $f = 70\%$–75%, i.e., soon after the "dead" layers are complete. Modes are observed at a significantly lower filling than anticipated from larger pore media. Also, in ^{4}He films and in partially filled large-pore media, the P-R mode energy, E_Q, consistently lies below the bulk liquid value at wave vectors in the maxon region, $Q \simeq 1.1\,\text{Å}^{-1}$. However, in partially filled 32 Å MCM-41 ($f = 90\%$) and 25 Å MPD gelsil ($f = 83\%$), an E_Q the same as the bulk value has been observed [14,28]. At partial fillings, the pores can also be full but at a reduced pressure [20].

These results suggest that the filling of small-pore media can be nonuniform. At partial fillings some regions are fully filled and bulklike while others have only a film. In 44 Å

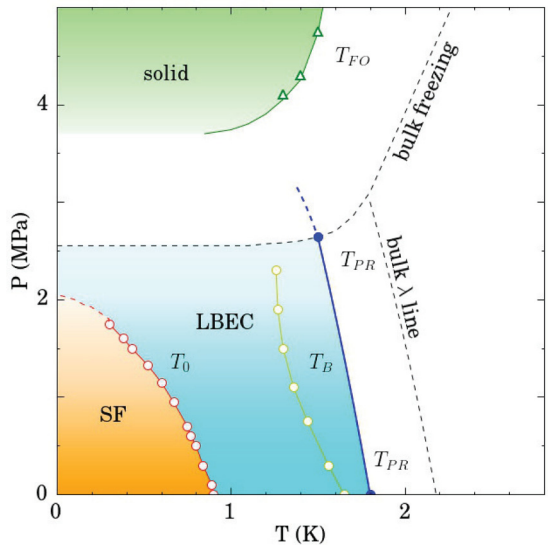

FIG. 13. Phase diagram of liquid ^{4}He in the present FSM-16 showing the localized Bose-Einstein condensation (LBEC) region (blue). The region interpreted as LBEC extends from temperature T_O to T_{PR}, where T_{PR} is the temperature at which P-R modes at $Q > 0.8$ Å^{-1} are no longer observed. Well defined P-R modes at wave vectors $Q > 0.8$ Å^{-1} exist only where there is BEC (i.e., $T_{\rm BEC} = T_{PR}$).

MPD gelsil a mode energy E_Q at $Q \simeq 1.1$ Å^{-1} below the bulk value was observed [15] at fillings $f = 84\%$ and $f = 95\%$. This suggests the presence of films or reduced pressure. In the present FSM, at filling N_2 ($f = 86\%$), an E_Q below the bulk value is also observed. An E_Q below the bulk value in the present FSM-16 could arise from a negative pressure in the FSM-16 or from significant scattering from the film component in nonuniform filling. We also observed modes at $f = 76\%$ ($N = 28$ mmol/g) in the present FSM. Mode energies are discussed further in Sec. IV C 1. The observation of modes at low fillings (e.g., 70%–75%) and of different E_Q in different small-pore media at similar partial fillings suggests nonuniform filling in small-pore media.

B. Phase diagram, liquid ^{4}He in FSM

Figure 1 shows the phase diagram of liquid ^{4}He in the pores of FSM. We have measured the temperature, T_{PR}, above which well-defined P-R modes in this liquid are no longer observed at higher wave vectors, $Q \gtrsim 0.8$ Å^{-1}. At SVP, $T_{PR} = 1.8$ K, and at $p = 26$ bars, $T_{PR} = 1.5$ K. Well-defined modes at higher wave vectors exist where there is BEC [12,19,22,52,53]. The temperature, T_{PR}, at which the modes are no longer observed can therefore be identified as $T_{\rm BEC}$, the onset temperature of BEC in the liquid. If $T_{\rm BEC}$ lies at a temperature above the critical temperature for superflow, T_C, the BEC at $T > T_C$ is interpreted as localized BEC (LBEC). In the LBEC region, the BEC is pictured as being localized to puddles or globules of BEC immersed within an otherwise normal liquid. The LBEC region lies in the temperature range $T_C < T < T_{\rm BEC}$.

If the T_O observed by Taniguchi *et al.* [21] and shown in Fig. 1 is interpreted as T_C, then the LBEC lies in the temperature range $T_O < T < T_{PR}$. A phase diagram with the LBEC region identified is shown in Fig. 13. At lower temperatures $T < T_O$, the BEC is interpreted as connected (extended) over long length scales, BEC that supports superflow observable in a torsional oscillator. LBEC in other porous media has been discussed extensively [7,8,12,17,19,21,22].

The superflow observed [21] in FSM is somewhat different from that observed in other porous media. In FSM, a small superfluid fraction, ρ_S/ρ, is observed at temperatures above T_O, up to a temperature T_B shown in Figs. 1 and 13. The temperature range $T_O < T < T_B$ was interpreted by Taniguchi *et al.* [21] as LBEC, but an LBEC that may not be fully localized, since the walls of FSM nanopores are smooth and may not fully localize the BEC. T_B is the highest temperature at which the small ρ_S/ρ was observed. T_B was interpreted as $T_{\rm BEC}$. Clearly, T_B and the $T_{\rm BEC} = T_{PR}$ agree well. Physically, we also anticipate that a $T_{\rm BEC}$ observed in a torsional oscillator will lie at or below $T_{\rm BEC}$ observed from P-R modes.

C. Phonon-roton and layer mode energies and widths

In this section we compare the P-R and layer mode energies and widths observed in FSM-16 with those observed in other porous media and previous measurements in FSM-16. The goal of the comparison is to place in perspective the P-R mode energies and widths observed here in FSM-16 at low temperature and as a function of temperature.

1. P-R mode energies and widths

In larger pore media, such as aerogel and Vycor [11,12,19], at full filling of the pores, the P-R mode energy and width at SVP is the same as in bulk liquid ^{4}He. This is both at low temperature and as a function of temperature up to T_λ. A broad layer mode at wave vectors 1.7 Å$^{-1} \leqslant Q \leqslant 2.3$ Å^{-1} is also observed as discussed below. At partial fillings, such as in aerogel [11] and on flat surfaces [45], the P-R mode energy E_Q lies somewhat below the bulk value at wave vectors in the maxon region (e.g., $E_Q = 1.15$ meV at $Q = 1.1$ Å^{-1} on graphite [45] compared with $E_Q = 1.18$ meV in bulk liquid [44]), and E_Q lies marginally above the bulk value at the roton wave vector [11], $Q = 1.95$ Å^{-1}, as if the density of the initial liquid layers is somewhat lower than the bulk value.

The data are less consistent in smaller pore media. In the present FSM-16 at filling $f = 86\%$, Fig. 7 shows that E_Q lies below the bulk value at $Q = 1.1$ Å^{-1} (i.e., $E_Q = 1.12$ meV at $Q = 1.1$ Å^{-1}) but is the same as bulk at $Q = 1.95$ Å^{-1}. In measurements not shown, E_Q at $Q = 1.1$ Å^{-1} depended on filling and E_Q increased with increasing filling.

This behavior is observed in some small-pore media but not in all. For example, in gelsil [15] of MPD 44 Å E_Q lies below the bulk value at maxon wave vectors at fillings of 84% and 95% (i.e., $E_Q = 1.1$ meV at $Q = 1.1$ Å^{-1} at $f = 84\%$) and E_Q is the same as that in the bulk at $Q = 1.95$Å^{-1}. In contrast, in Geltech [14] of 25 Å MPD at $f = 83\%$ and in MCM-41 nanopores of 32 Å diameter [28], an E_Q the same as the bulk E_Q at all Q is reported. The gelsils have a broad distribution of pore diameters. For example, in 34 Å MPD gelsil [16], the

distribution is approximately Gaussian peaked at 34 Å with a FWHM of 40 Å. In contrast, MCM-41 nanopores have a narrow distribution of pore diameters.

In the present FSM-16, a large mode width at $T \to 0$ at $f = 86\%$ is observed. The mode width decreased with increasing filling. The decrease of $2\Gamma_Q$ with filling suggested a mode width at $Q = 1.1$ Å^{-1} of $2\Gamma_Q \simeq 0.05$ meV at full filling at SVP. The width at the $Q = 1.95$ Å^{-1} is more difficult to determine because of the presence of the layer mode. At pressure $P = 25$ bars, a finite roton width at full filling of $2\Gamma_Q = 0.12$ meV is indicated.

A large P-R mode width at low temperature was also reported [15] in 44 Å MPD gelsil, e.g., at $Q = 1.1$ Å^{-1}, $2\Gamma_Q \simeq 0.22$ meV at $f = 84\%$ and 0.08 meV at $f = 95\%$. In contrast, in MCM-41 nanopores [28] of 32 Å diameter at filling $f = 90\%$ and in 25 Å^{-1} gelsil [14] at SVP the widths are small at low temperature. In MCM-41, the width also remains relatively small at higher temperature, e.g., $2\Gamma_Q = 0.08$ meV at 1.5 K, approximately twice the bulk liquid value. An E_Q the same as in bulk and a small mode width in MCM-41 and 25 Å^{-1} gelsil suggests nonuniform filling in these media at SVP with most regions fully filled and others little filled and not contributing to the mode response.

These comparisons show that at partial fillings, an E_Q below the bulk value at $Q \simeq 1.1$ Å^{-1} and large P-R mode widths at low temperature have been observed previously but are not observed universally in all small-pore media. The large width could arise, in part, from a distribution of liquid densities at partial fillings. The significant increase of the widths with increasing temperature in the present FSM-16 suggests there are thermal processes intrinsic to the confined liquid. These processes could involve a distribution of mode energies that produce a finite width at $T \to 0$ K and an enhanced temperature dependence.

The present results can be most directly compared with those of Prisk *et al.* [18] and Bryan *et al.* [38] for liquid ^{4}He also confined in 28 Å FSM-16. The present FSM-16 sample should be very similar to that used in Refs. [18] and [38] since both samples were made to the same specifications by the same manufacturer. At fillings of 33.4 mmol/g and 37.7 mmol/g, Prisk *et al.* [18] report an E_Q at $Q = 1.15$ Å^{-1} that lies very significantly below the bulk value and significantly below the values reported here. They also observe large widths at low temperature, e.g., a $2\Gamma_Q \simeq 0.30$ meV at $Q = 1.15$ Å^{-1} and $2\Gamma_Q \simeq 0.60$ meV at $Q = 1.95$ Å^{-1} (see Figs. 8–10 of Ref. [18]). The E_Q has no filling dependence between fillings of 33.4 mmol/g and 37.7 mmol/g.

Mode energies, E_Q, equal to the bulk liquid energies are reported at 43.0 mmol/g and 46.4 mmol/g (with no filling dependence between 43.0 mmol/g and 46.4 mmol/g). Similarly, at a filling of 47 mmol/g, Bryan *et al.* [38] report an E_Q and $2\Gamma_Q$ as a function of temperature that is the same as those in bulk liquid ^{4}He.

References [18] and [38] appear to use an isotherm taken at 4.2 K as a guide to filling. This isotherm indicates full filling at 47 mmol/g. However, isotherms taken at several temperatures, as shown here in Fig. 2, and particularly that at 2.5 K indicate full filling at approximately 37 mmol/g. At higher temperature (e.g., 4.2 K) where the vapor pressure is high, some of the ^{4}He that goes into the cell goes into the vapor above the FSM-16 as well as in the FSM-16. Figure 2 shows that at 3.8 K some 5 mmol/g has gone into the vapor in the present cell. If a cell is filled to 47 mmol/g at 4.2 K and then cooled to 0.5 K, say, the ^{4}He that was in the vapor condenses to liquid. If the total ^{4}He added at 4.2 K exceeds full filling at low temperature, then the excess will condense to bulk liquid in the cell at low temperature. This bulk liquid produces a strong bulklike scattering intensity. At fillings of 43 mmol/g and 46.4 mmol/g, from the temperature dependence of the isotherms shown in Fig. 2, the FSM-16 may be overfilled by several mmol/g at low temperature (e.g., $T < 2.0$ K). Thus at fillings of 43 mmol/g and 46.4 mmol/g a strong signal from the condensed bulk liquid would be observed. It would be interesting to test this suggestion in future measurements.

2. *Layer modes*

In the present FSM-16, we observe a broad layer mode at wave vectors 1.7 Å^{-1} $\leqslant Q \leqslant$ 2.3 Å^{-1}. The mode lies below the P-R mode and has a roton-like dispersion with a minimum energy of $\Delta_L = 0.54 \pm 0.02$ meV and FWHM $= 0.4$ meV at SVP. The mode is robust and approximately independent of temperature up to $T = 1.6$ K. A layer mode is widely observed in other porous media, for example in Vycor [12] with $\Delta_L = 0.55 \pm 0.01$ meV, in aerogel [11,12] with $\Delta_L = 0.63 \pm 0.01$, and in 25 Å MPD gelsil and 47 Å MCM-41 [17] with $\Delta_L = 0.60 \pm 0.02$ meV all at SVP. In gelsil [54], a layer mode largely independent of temperature up to 1.6 K was also observed.

In Vycor and 25 Å MPD gelsil the specific heat at intermediate temperatures appears to arise from exciting the layer mode (rather than exciting the P-R mode as in the bulk liquid). For example, fits of the Landau expression for the specific heat arising from a roton-like mode to the observed C_V yield a minimum energy of 0.53 meV and 0.54 meV in Vycor [1,55] and in 25 Å MPD gelsil [8], respectively. These values are in reasonable agreement with the layer mode minima $\Delta_L = 0.55 \pm 0.01$ meV and $\Delta_L = 0.60 \pm 0.02$ meV quoted above. To check that the specific heat of FSM-16 observed by Taniguchi *et al.* [21] also arises from exciting the layer mode, we fitted the Landau expression to the specific heat of FSM-16 in the temperature range $0.7 \leqslant T \leqslant 1.3$ K. The best-fit minimum energy of a roton-like dispersion curve was 0.52 meV at 0.3 bars, in good agreement with the layer mode minimum energy of $\Delta_L = 0.54 \pm 0.02$ that we observe in the present FSM-16.

D. Dimensions of ^{4}He in FSM-16

What do $S(Q, E)$ and the P-R mode energies, E_Q, tell us about the effective dimensions of liquid ^{4}He in FSM-16? Is the liquid 1D-, 2D-, or 3D-like?

Following the deposit of the "dead" (solid) layers on the pore walls, ^{4}He liquid is deposited in cylindrical shells of liquid [30–32,56,57]. The liquid density peaks at the center of the shell. There is a density minimum between the shells. FSM-16 of diameter 28 Å (liquid diameter of 18 Å) is completely filled by the "dead" layers, two liquid shells, and a

density peak at the center of the pore. The superfluid density and Bose-Einstein condensation in the liquid shells scale as expected for a 2D fluid [32]. 3D scaling is found at larger pore diameters [32]. At $f = 86\%$, most of the nanopore is filled as described above separated by regions having only thin liquid films. At this filling, $S(Q, E)$ is well fitted by a DHO and the P-R mode energy has the character expected for thick films and confined bulk liquid ^{4}He.

To discuss predictions for a 1D liquid, we note that Krotscheck and Miller [58] and Bertaina *et al.* [37] have evaluated $S(Q, E)$ and E_Q explicitly for a freestanding, 1D line of ^{4}He atoms. Because of the similarity of Bose and Fermi gases in 1D [59], the calculated $S(Q, E)$ shows some character of an interacting Fermi gas. Specifically, there is a particle-hole band and $S(Q, E)$ lies predominantly within the band. Within $S(Q, E)$ there is a collective mode. The energy, E_Q, of the collective mode is qualitatively described by the Feynman relation $E_Q = (\hbar Q)^2/2mS(Q)$, where $S(Q)$ is the static structure factor. E_Q is dictated by $S(Q)$. At higher linear densities, ρ_0, the 1D liquid becomes solid-like and $S(Q)$ develops Bragg-like peaks at $Q = 2\pi n/a$ with $S(2\pi n/a) \propto N^{1-2n^2K}$. K is the Luttinger liquid parameter, which is small at high linear density ($\rho_0 = 0.2$–0.3 Å^{-1}). $S(Q)$ is especially large at $Q = 2\pi/a$. This drives E_Q to zero at $Q = 2\pi/a$.

To compare predictions for 1D directly with the present measurements we must identify the corresponding 1D liquid density, ρ_0. For example, the equilibrium, zero-pressure density of an ideal, freestanding 1D line of ^{4}He is very small [37,58,60], $\rho_0(\text{eq}) \simeq 0.036$ Å^{-1}. Similarly, at equilibrium the density of a 1D line of ^{4}He confined in a narrow nanopore of diameter 6 Å is small [33], $\rho_0(\text{eq}) \simeq 0.108$ Å^{-1} (interatom spacing $a = 9.26$ Å). These densities are much less than that of the liquid ^{4}He in FSM-16. If the 1D line in the nanopore is compressed to interatom spacing $a = 3.75$ ($\rho_0 = 0.267$ Å^{-1}), the corresponding 3D liquid density in the nanopore is $\rho = 0.0212$ Å^{-3}, close to the 3D density of bulk liquid ^{4}He at SVP ($\rho = 0.0218$ Å^{-3}), the density of the liquid in the present FSM-16. In 1D liquids at this density (i.e., $\rho_0 = 0.25$–0.30 Å^{-1}), $S(Q)$ is very large at $Q = 2\pi/a$. The corresponding mode energy, E_Q, goes to zero at $Q = 2\pi/a$.

In 1D $Q = 2\pi/a$ corresponds to the roton wave vector, Q_R, and E_Q to the roton mode energy. To have the roton wave vector $Q_R = 2\pi/a$ at the observed value, $Q_R = 1.95$ Å^{-1}, a 1D spacing of $a = 3.22$ Å ($\rho_0 = 0.31$ Å^{-1}) is required. This 1D spacing is consistent with that selected above. The corresponding 1D roton mode energy, E_Q, at $Q_R = 2\pi/a$ will be zero [37]. In contrast, we observe an E_Q equal to the bulk 3D liquid roton energy within precision. We do not observe a roton mode energy $E_Q \to 0$ at the roton wave vector. Thus we conclude that the observed $S(Q, E)$ and mode energy, E_Q, are quite different from that expected for 1D ^{4}He. The liquid in 28 Å diameter FSM-16 is not 1D-like but rather 2D- to 3D-like.

V. CONCLUSION

We have measured the dynamical structure factor (DSF) and the characteristic phonon-roton (PR) modes of liquid ^{4}He confined in nanoporous FSM-16. FSM-16 is an array of individual, parallel, and straight nanopores of diameter 28 Å. Most other porous media consist of interconnected, rough-walled pores so that the confined ^{4}He forms an interconnected disordered 3D liquid. The walls of FSM-16 are also smoother than those of other media (reduced disorder).

The goal is to determine whether the Bose-Einstein condensation (BEC) in the liquid ^{4}He forms a localized BEC (LBEC) phase induced by disorder. We find that it does and we determine the temperature range of the LBEC phase at two pressures. The LBEC region is compared with existing measurements [21] of the superfluid phase in FSM-16. A second goal is to determine the effective dimensions (D) of the liquid in the nanopores, whether it is 1D-, 2D-, or 3D-like. In terms of the dynamics, we find the liquid is 2D-3D-like and not 1D-like. The observed PR mode energies are very different from that predicted [37,58] for a 1D Bose fluid.

Specifically, at low temperature, e.g., $T = 0.43$ K, well-defined P-R modes that have clearly resolvable width are observed. As temperature is increased the mode widths increase, substantially at SVP but not sufficient to be further resolved at 26 bars. At 1.4 K and SVP, the mode widths are 10–15 times the bulk SVP value.

Well-defined P-R modes at wave vectors beyond the phonon region ($Q \geqslant 0.8$ Å^{-1}) are observed up to a temperature $T_{PR} = 1.8$ K at SVP and $T_{PR} = 1.5$ K at 26 bars. Since P-R modes are observed at $Q \geqslant 0.8$ Å^{-1} only where there is BEC, the temperature T_{PR} is identified as the onset temperature of BEC, $T_{\text{BEC}} = T_{PR}$. T_{BEC} lies well above the onset temperature of superfluidity, T_O, observed in torsional oscillator measurements (e.g., $T_O = 0.9$ K at SVP). This indicates that there is temperature range, $T_O \leqslant T \leqslant T_{\text{BEC}}$, where there are disconnected puddles of localized BEC (LBEC). In this range there is LBEC but no superflow across the sample in FSM-16 (straight nanopores), as observed in the interconnected pores of Vycor and gelsil [7,8,12,14,19]. The T_{BEC} identified here from P-R modes agrees reasonably well with the T_{BEC} identified by Taniguchi *et al.* [21] from reduced superflow in FSM-16.

ACKNOWLEDGMENTS

It is a pleasure to acknowledge the support of the Institut Laue-Langevin and the valuable assistance of O. Losserand, X. Tonon, and S. Baudouin with the experiments at ILL. We thank Professor Junko Taniguchi for providing the FSM sample and critical data on the sample. H.R.G. acknowledges the support of the Theory Group at ILL, where much of the manuscript was written. This work was supported in part by the DOE, Office of Basic Energy Sciences, under Contract No. ER46680.

[1] D. F. Brewer, in *The Physics of Liquid and Solid Helium, Part II*, edited by K. H. Benneman and J. B. Ketterson (Wiley, New York, 1978), p. 573.

[2] J. D. Reppy, J. Low Temp. Phys. **87**, 205 (1992).

[3] M. H. W. Chan, M. Mulders, and J. D. Reppy, Phys. Today **49**(8), 30 (1996).

[4] M. H. W. Chan, K. I. Blum, S. Q. Murphy, G. K. S. Wong, and J. D. Reppy, Phys. Rev. Lett. **61**, 1950 (1988).

[5] G. M. Zassenhaus and J. D. Reppy, Phys. Rev. Lett. **83**, 4800 (1999).

[6] F. Albergamo, H. R. Glyde, D. R. Daughton, N. Mulders, J. Bossy, and H. Schober, Phys. Rev. B **69**, 014514 (2004).

[7] K. Yamamoto, H. Nakashima, Y. Shibayama, and K. Shirahama, Phys. Rev. Lett. **93**, 075302 (2004).

[8] K. Yamamoto, Y. Shibayama, and K. Shirahama, Phys. Rev. Lett. **100**, 195301 (2008).

[9] R. M. Dimeo, P. E. Sokol, C. R. Anderson, W. G. Stirling, K. H. Andersen, and M. A. Adams, Phys. Rev. Lett. **81**, 5860 (1998).

[10] C. R. Anderson, W. G. Stirling, K. H. Andersen, P. E. Sokol, and R. M. Dimeo, Physica B **276-278**, 820 (2000).

[11] B. Fåk, O. Plantevin, H. R. Glyde, and N. Mulders, Phys. Rev. Lett. **85**, 3886 (2000).

[12] O. Plantevin, B. Fåk, H. R. Glyde, N. Mulders, J. Bossy, G. Coddens, and H. Schober, Phys. Rev. B **63**, 224508 (2001).

[13] C. R. Anderson, K. H. Andersen, W. G. Stirling, P. E. Sokol, and R. M. Dimeo, Phys. Rev. B **65**, 174509 (2002).

[14] O. Plantevin, H. R. Glyde, B. Fåk, J. Bossy, F. Albergamo, N. Mulders, and H. Schober, Phys. Rev. B **65**, 224505 (2002).

[15] F. Albergamo, J. Bossy, J. V. Pearce, H. Schober, and H. R. Glyde, Phys. Rev. B **76**, 064503 (2007).

[16] J. Bossy, J. V. Pearce, H. Schober, and H. R. Glyde, Phys. Rev. Lett. **101**, 025301 (2008).

[17] J. Bossy, J. Ollivier, H. Schober, and H. R. Glyde, Europhys. Lett. **98**, 56008 (2012).

[18] T. R. Prisk, N. C. Das, S. O. Diallo, G. Ehlers, A. A. Podlesnyak, N. Wada, S. Inagaki, and P. E. Sokol, Phys. Rev. B **88**, 014521 (2013).

[19] H. R. Glyde, O. Plantevin, B. Fak, G. Coddens, P. S. Danielson, and H. Schober, Phys. Rev. Lett. **84**, 2646 (2000).

[20] F. Albergamo, J. Bossy, P. Averbuch, H. Schober, and H. R. Glyde, Phys. Rev. Lett. **92**, 235301 (2004).

[21] J. Taniguchi, R. Fujii, and M. Suzuki, Phys. Rev. B **84**, 134511 (2011).

[22] S. O. Diallo, R. T. Azuah, D. L. Abernathy, J. Taniguchi, M. Suzuki, J. Bossy, N. Mulders, and H. R. Glyde, Phys. Rev. Lett. **113**, 215302 (2014).

[23] W. Thomlinson, J. A. Tarvin, and L. Passell, Phys. Rev. Lett. **44**, 266 (1980).

[24] N. Wada, J. Taniguchi, H. Ikegami, S. Inagaki, and Y. Fukushima, Phys. Rev. Lett. **86**, 4322 (2001).

[25] N. Wada, Y. Minato, T. Matsushita, and M. Hieda, J. Phys. Soc. Jpn. **77**, 111012 (2008).

[26] N. Wada, Y. Minato, T. Matsushita, and M. Hieda, J. Low Temp. Phys. **162**, 549 (2011).

[27] J. Taniguchi, Y. Aoki, and M. Suzuki, Phys. Rev. B **82**, 104509 (2010).

[28] F. Albergamo, J. Bossy, H. R. Glyde, and A. J. Dianoux, Phys. Rev. B **67**, 224506 (2003).

[29] A. Del Maestro and I. Affleck, Phys. Rev. B **82**, 060515(R) (2010).

[30] A. Del Maestro, M. Boninsegni, and I. Affleck, Phys. Rev. Lett. **106**, 105303 (2011).

[31] B. Kulchytskyy, G. Gervais, and A. Del Maestro, Phys. Rev. B **88**, 064512 (2013).

[32] L. V. Markić and H. R. Glyde, Phys. Rev. B **92**, 064510 (2015).

[33] L. Vranješ Markić, H. Vrcan, Z. Zuhrianda, and H. R. Glyde, Phys. Rev. B **97**, 014513 (2018).

[34] M. A. Cazalilla, R. Citro, T. Giamarchi, E. Orignac, and M. Rigol, Rev. Mod. Phys. **83**, 1405 (2011).

[35] A. Imambekov, T. L. Schmidt, and L. I. Glazman, Rev. Mod. Phys. **84**, 1253 (2012).

[36] T. Eggel, M. A. Cazalilla, and M. Oshikawa, Phys. Rev. Lett. **107**, 275302 (2011).

[37] G. Bertaina, M. Motta, M. Rossi, E. Vitali, and D. E. Galli, Phys. Rev. Lett. **116**, 135302 (2016).

[38] M. S. Bryan, T. R. Prisk, T. E. Sherline, S. O. Diallo, and P. E. Sokol, Phys. Rev. B **95**, 144509 (2017).

[39] J. V. Pearce, S. O. Diallo, H. R. Glyde, R. T. Azuah, T. Arnold, and J. Z. Larese, J. Phys. Condens. Matter **16**, 4391 (2004).

[40] E. F. Talbot, H. R. Glyde, W. G. Stirling, and E. C. Svensson, Phys. Rev. B **38**, 11229 (1988).

[41] G. A. Csáthy, J. D. Reppy, and M. H. W. Chan, Phys. Rev. Lett. **91**, 235301 (2003).

[42] K. Beauvois, C. E. Campbell, J. Dawidowski, B. Fåk, H. Godfrin, E. Krotscheck, H.-J. Lauter, T. Lichtenegger, J. Ollivier, and A. Sultan, Phys. Rev. B **94**, 024504 (2016).

[43] H. R. Glyde, Rep. Prog. Phys. **81**, 014501 (2018).

[44] M. R. Gibbs, K. H. Andersen, W. G. Stirling, and H. Schober, J. Phys. Condens. Matter **11**, 603 (1999).

[45] H. J. Lauter, H. Godfrin, V. L. P. Frank, and P. Leiderer, Phys. Rev. Lett. **68**, 2484 (1992).

[46] A. D. B. Woods and E. C. Svensson, Phys. Rev. Lett. **41**, 974 (1978).

[47] K. H. Andersen, W. G. Stirling, R. Scherm, A. Stunault, B. Fåk, H. Godfrin, and A. J. Dianoux, J. Phys.: Condens. Matter **6**, 821 (1994).

[48] K. H. Andersen, W. G. Stirling, H. R. Glyde, R. T. Azuah, A. D. Taylor, S. M. Bennington, Z. A. Bowden, and I. Bailey, Phys. B (Amsterdam, Neth.) **197**, 198 (1994).

[49] K. H. Andersen and W. G. Stirling, J. Phys.: Condens. Matter **6**, 5805 (1994).

[50] B. Fåk, T. Keller, M. E. Zhitomirsky, and A. L. Chernyshev, Phys. Rev. Lett. **109**, 155305 (2012).

[51] H. Godfrin, V. Lauter-Pasyuk, H. Lauter, and P. Leiderer (unpublished).

[52] J. Gavoret and P. Nozières, Ann. Phys. **28**, 349 (1964).

[53] H. R. Glyde and A. Griffin, Phys. Rev. Lett. **65**, 1454 (1990).

[54] J. Bossy, H. Schober, and H. R. Glyde, Phys. Rev. B **91**, 094201 (2015).

[55] D. F. Brewer, A. J. Symonds, and A. L. Thomson, Phys. Rev. Lett. **15**, 182 (1965).

[56] E. Krotscheck, Phys. B (Amsterdam, Neth.) **280**, 59 (2000).

[57] M. Rossi, D. E. Galli, and L. Reatto, Phys. Rev. B **72**, 064516 (2005).

[58] E. Krotscheck and M. D. Miller, Phys. Rev. B **60**, 13038 (1999).

[59] M. Girardeau, J. Math. Phys. **1**, 516 (1960).

[60] M. Boninsegni and S. Moroni, J. Low Temp. Phys. **118**, 1 (2000).

[61] J. Taniguchi (private communication).